

A Noise-free and Jitter-less Cavity System to Distribute Clocks over 10GHz

Hatsuhiro Kato*, Takaya Kohori, Eiichi Kondoh, Tetsuya Akitsu and Hatsuyoshi Kato

Abstract—We discuss a novel method using a cavity to deliver a high frequency clock in ULSI systems. This method can distribute global clock over 10GHz without skew and EMI noise. Because the cavity can be formed by a usual metallization or its extended process, it will be realized easier compared with other emerging technology such as photoelectric circuit. However, the cavity is thin and affected by energy dissipation on cavity walls. Considering energy dissipation, we discuss features of a cavity system.

Index Terms—Cavity, clocks, metallization, resonant clocking, Interconnect, LSI

I. INTRODUCTION

THE clock frequency in ULSI systems increases year by year and will exceed 10GHz and the die size will be larger loading a huge complicated system. Therefore, it turns out to be difficult to distribute global clock over a whole area of a ULSI by a conventional bus line because of the high-frequency effects such as propagation delay or noise emission [1,2]. Especially, the frequency discrepancy between the global and the local clocks is concerned with the data transfer rate between system blocks. Recently, several proposal to reduce the discrepancy is discussed, for example, a system using a dipole antenna [3,4,5] or optoelectronics interconnects [6]. If the clock frequencies in a ULSI chip increases over 10GHz, the frequency discrepancy will be a serious problem. We proposed a novel cavity system to distribute the global clock. This system uses the standing wave formed in a cavity as a clock signal and realizes jitter- and noise-free clock distribution to internal intellectual property (IP) blocks [7,8]. If a thick insulator film over 10 μ m is possible, a cavity for clock delivery system can be fabricated on top of the ULSI system.

Compared with a system using the optoelectronics interconnection, the cavity system requires fewer loads for process technology and does not demand an exceptional technical breakthrough of a cost. A method also using a standing wave on parallel transmission lines was proposed [9, 10], but this system is to be a source of EMI noise at a high

frequency since transmission lines are opened. On the other hand, our cavity system encloses magnetic waves and is principally free from noise generation. Moreover, our method does not require buffering gates to compensate the signal damping along the bus line. This feature is technically feasible to reduce the clock skew.

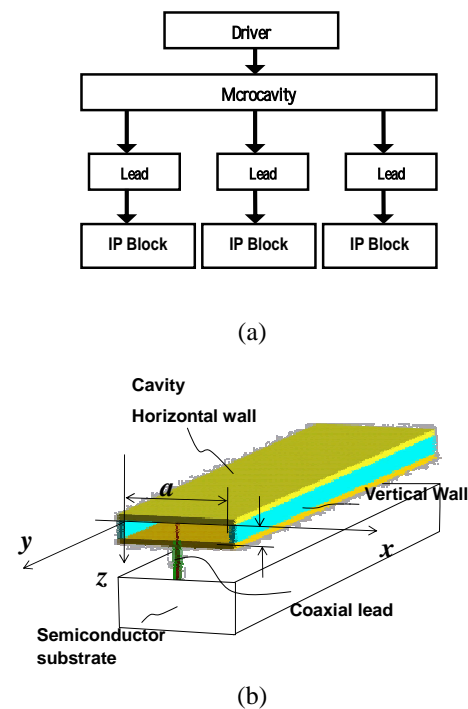


Fig. 1. A block diagram of proposed clock distribution system (a) and a schematic structure of cavity on a semiconductor substrate (b).

II. SYSTEM CONFIGURATION AND STRUCTURE

In Fig. 1, a block diagram (a) and a schematic structure (b) of the proposed system are shown. A cavity is driven by a circuit on a substrate or a planar Gun diode to generate a standing wave of the microwave. The signal in a cavity is led to each IP block on a substrate by microwave leads. Because the frequency of a standing wave does not depend on the location, a clock generated by a standing wave has no skew, principally. If the resonance curve of a cavity has a sharp peak, the frequency fluctuation of the clock or jitter will be suppressed significantly. Therefore, an ideal global clock can be generated by use of a cavity system.

Manuscript received 10th November 2005; revised 25th April 2006.

H. Kato*, T. Kohori, E. Kondoh and T. Akitsu are with University of Yamanashi, 4-3-44 Takeda, Kofu, 400-8511, Japan (H. Kato* is corresponding author to provide phone: +49-55-220-8692; fax: +49-55-220-8779; e-mail: kato@yamanashi.ac.jp)

H. Kato is with National College of Tomakomai, 433, Nishikioka, Tomakomai, 059-1275, Japan (e-mail: kato@gt.tomakomai-ct.ac.jp)

A schematic of the cavity structure is shown in Fig.1 (b) with a cross section of a microwave lead formed on a semiconductor substrate. The top and bottom horizontal walls of a cavity can be fabricated by a standard metallization process and the vertical walls can be formed by a via process. Because the direction of currents on the side walls is vertical, an array of via pillars is applicable instead of continuum walls.

A typical dimension of a cavity is 3.2mm in width a , which is determined by wave length of microwave, and 12mm in length b , being comparable to the chip size. The thickness c is assumed to be $10\mu\text{m}$. In the figure the vertical scale is magnified for convenience sake to show the inner structure. The lead should be located where the amplitude of the standing wave has the same magnitude, for example, the maximum points of the amplitude or the points a $1/8$ of the wave length away from the maximum points.

When the frequency reaches 30GHz, the skin depth becomes about $0.5\mu\text{m}$, which is less than a typical metal thickness of $1\mu\text{m}$ and a magnetic wave scarcely leaks from the cavity. For the higher frequencies the skin depth becomes less thinner, therefore the cavity system produces no EMI noise compared with transmission lines. In this paper, the thickness of cavity walls is assumed to be much larger than the skin depth.

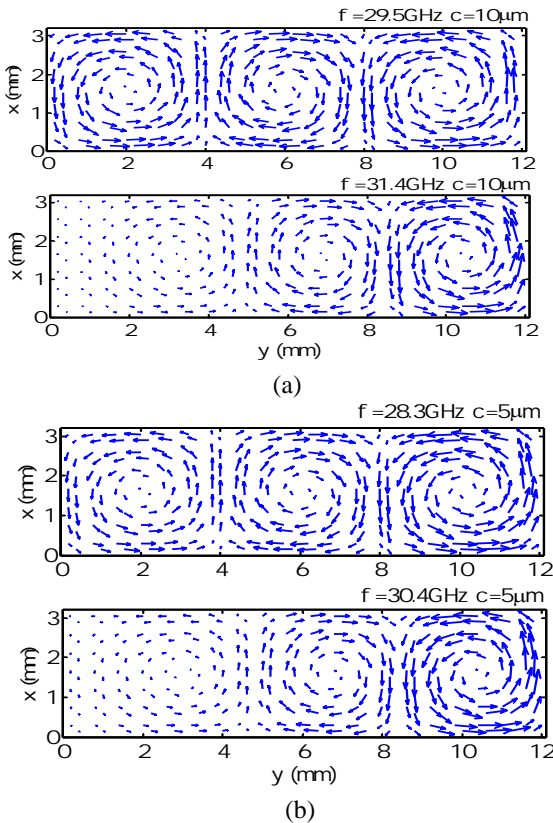


Fig.2. The vector map of a magnetic field for $c = 10\mu\text{m}$ (a) and $c = 5\mu\text{m}$ (b), which are obtained by the FEM with consideration of the energy dissipation on metallic walls. The other cavity dimensions are $a \times b = 3.2 \times 12\text{mm}$.

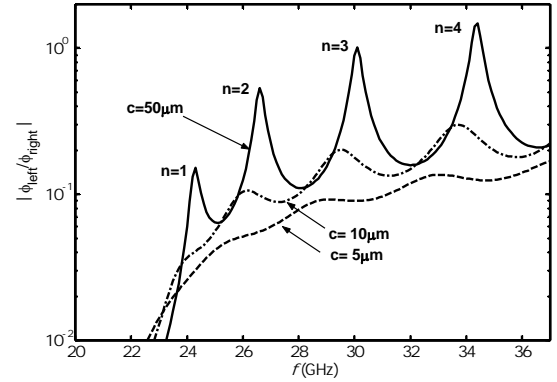


Fig.3. The resonance curves of a cavity for various thickness c , which are obtained by the FEM with consideration of a energy dissipation on metallic walls. The other cavity dimensions are the same for Fig.2.

III. FEATURES OF CAVITY

A. Resonance Property

When the energy dissipation is negligible, the resonance frequency f_0 of TE wave is given by

$$f_0 = \frac{1}{2} \sqrt{\frac{1}{\epsilon\mu} \left(\frac{1}{a^2} + \frac{n^2}{b^2} \right)}. \quad (1)$$

Here, the inside dimensions of a cavity are $a \times b \times c$, ϵ and μ are dielectric constant and susceptibility of a filling material. The mode indexes along the direction of a , b and c are assumed to be 1, n and 0. This means the field strength along the thickness c is uniform and the number of antinodes along axis of a (or b) is one (or n). The cutoff frequency f_{cr} is expressed by $f_{cr} = 1/2a(\epsilon\mu)^{1/2}$, which is the minimum frequency over which the microwave can penetrates and its value is $f_{cr} = 23.7\text{GHz}$ when the filler is SiO_2 and the width of the cavity is $a = 3.2\text{mm}$. The detail of the resonance curve is influenced by the dielectric loss due to the filler and the Joule heat generated on the metallic walls. Therefore, the resonance frequency becomes smaller than the value given by (1). The dominant reason for the dissipation is the Joule heat because the cavity thickness c is very thin,

To analyze the effect of the energy dissipation, we modified FEM (Finite Element Method) using vector base functions [8]. Because the Joule heat is caused by the induced current due to the rotation of a magnetic field, we chose a magnetic field as a field vector and developed a formulation of FEM (see appendix A). In Fig. 2, vector diagrams of a magnetic field in a cavity is shown for thicknesses of $c = 10\mu\text{m}$ (a) and $c = 5\mu\text{m}$ (b). The x -axis (y -axis) is set along the width (length) direction and the midpoint of the thickness is selected as $z = c/2$. The material of the cavity wall is assumed to be copper (Cu) and the filler is to be SiO_2 . Because the cavity is driven at the midpoint of the right edge (*i.e.* $y = b$), the field strength on the left edge (*i.e.* $y = 0$) is a measure of whether the microwave can penetrate into the cavity or not. As shown in Fig.2 (a), when the driving

frequency is $f = 29.5\text{GHz}$, a standing wave of three antinodes exists. On the other hand, when the driving frequency changes to $f = 31.4\text{GHz}$, the field scarcely penetrates to the left. This is caused by the interference of the input and the reflected waves. The same phenomena is shown in Fig.2 (b) for $c = 5\mu\text{m}$.

In Fig. 3 a sort of the resonance curve is shown for various thicknesses c , which is the relation between the driving frequency f and the ratio of the input strength of a magnetic field, ϕ_{right} , applied on the right edge and the strength of a magnetic field, ϕ_{left} , at the left edge. The larger the value of $\phi_{\text{left}}/\phi_{\text{right}}$, the deeper the magnetic field penetrates into the cavity. A driving frequency $f = 29.5\text{GHz}$ in Fig.2 (a) corresponds to a peak labeled $n = 3$ and $c = 10\mu\text{m}$ in Fig. 3. The frequency is less than that of 30.4GHz obtained by equation (1) for $n = 3$. This frequency shift is involved by the energy dissipation as discussed in appendix A, where the resonance frequency $\omega_R (= 2\pi f_R)$ is related to the Q factor by (A10). The vector map for $f = 31.4\text{GHz}$ in Fig.2 (a) corresponds to a valley of resonance curve in Fig. 3. The same correspondence exists between Fig. 2 (b) and Fig. 3.

In Fig. 3 the peak of $n = 1$ becomes invisible as the thickness c decreases, which is caused by the spreading and the shift of the resonance peak. The resonance curve does not exist in the region less the cutoff frequency $f_{\text{cr}} = 23.7\text{GHz}$. However, the cutoff frequency and the resonance curve can be shifted to lower frequencies by adjusting the cavity dimensions. If the width a is 7.59mm , the frequency f_{cr} becomes 10GHz . The optimum dimensions are fixed according to a necessary frequency and the layout of IP blocks.

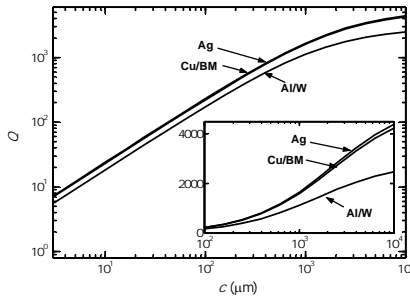


Fig. 4. The dependence of Q -factor on the cavity depth c for various cavity walls for $n = 3$. The cavity dimensions are $a \times b = 12\text{mm} \times 3.2\text{mm}$.

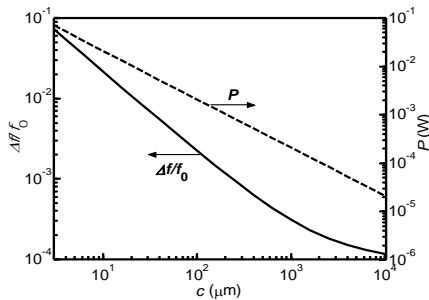


Fig. 5. The dependence of the jitter $\Delta f/f_0$ and the Joule heat power P on the cavity depth c for a cavity made by Cu/BM. The cavity dimensions are $a \times b = 12 \times 3.2\text{mm}$. The voltage between the upper

and the lower plates is $V_m = 0.33\text{V}$.

B. Resonance Peak and Cavity Thickness

Due to the skin effect, induced currents on a cavity wall tend to concentrate at the surface. Moreover, the metallic layer in the ULSI system is covered by a barrier metal (BM) of a large resistance. Therefore, the BM might enhance the energy dissipation and spread the peak width of the resonance curve. Criticizing the Q factor, which is a measure of sharpness of the resonance peak, we considered an influence of the BM on the resonance.

To estimate the influence of the Joule heat due to the induced currents on cavity walls, we define an effective sheet resistance R_{eff} with respect to the energy dissipation as discussed in Appendix B. An effective sheet resistance R_{eff} is for a metallic layer with BM, which is expressed by

$$R_{\text{eff}} = \frac{r}{\sigma_M \delta_M} \frac{(1+r)^2 e^{2d/\delta_B} - (1-r)^2 e^{-2d/\delta_B} + 2(1-r^2) \sin \frac{2d}{\delta_B}}{(1+r)^2 e^{2d/\delta_B} + (1-r)^2 e^{-2d/\delta_B} - 2(1-r^2) \cos \frac{2d}{\delta_B}} \quad (2)$$

Here, d and σ_B are the thickness and the conductance of BM, δ_B and δ_M are the skin depth defined by $\delta_B = 1/(\pi f \mu \sigma_B)^{1/2}$ and $\delta_M = 1/(\pi f \mu \sigma_M)^{1/2}$, respectively. The ratio r is defined by $r = (\sigma_M/\sigma_B)^{0.5}$. To derive (2) we assume that the skin depth is sufficiently smaller than the thickness of the cavity wall.

The Q factor is defined by $Q = 2\pi f_0 U/P_J$, with U the energy stored in the cavity and P_J , the power loss due to the Joule heat. This expression can be derived from a model where the oscillation of the cavity is mapped into a damping oscillator within a framework of FEM as discussed in Appendix A. According to this modeling we obtain an expression for the Q factor:

$$Q = \frac{2\pi f_0 \mu abc (b^2 + a^2 n^2)}{(R_{\text{HU}} + R_{\text{HL}})(b^2 + n^2 a^2) ab + 4R_V (b^3 + n^2 a^3) c}, \quad (3)$$

where R_{HU} (R_{HL}) and R_V are sheet resistances of the upper (lower) horizontal plate and vertical plate of cavity walls, respectively. These values are derived from (2).

According to equation (3), the dependence of Q on the cavity thickness c is shown in Fig. 4. The dimensions of a cavity are the same used in Fig.2 (a) and (b). The labels in the figure indicate the cavity material. The label Ag is for silver which has the large conductance and widely used for the cavity material, Cu/BM is for the copper (Cu) with the BM of tantalum (Ta) film with 20nm thickness. The difference of conductance between Ag and Cu is about 10% and this difference is scarcely visible in the logarithmic scale. The difference can be confirmed through the insertion with the axis of arithmetic scale. The curve with the label Al/W is for aluminum (Al) cavity using a tungsten plug for a via hole. The Ta film of 20nm thickness is also settled for the BM. The process of Al/W is well established and has a cost advantage, but large resistance

of W may cause the degradation of the Q factor. However, the area of the vertical walls made by the W plug is less than that of the horizontal aluminum (Al) walls and the influence of the tungsten (W) is not serious for $c < 1\text{mm}$.

The feature of a driving circuit is most important to suppress the jitter or fluctuation of the clock frequency. If a driving circuit has a sufficient response, the remaining factor to suppress the jitter is a sharpness of the resonance peak, which can be scaled by the Q factor. Assuming that a driving circuit detects $1/4$ of the width of the resonance peak, we obtained the relation between the Q factor and the jitter of the clock frequency Δf :

$$\frac{\Delta f}{f_0} \approx \frac{1}{2Q} + \frac{7}{16Q^2}. \quad (4)$$

A detail of derivation to obtain (4) is given in Appendix A. In Fig. 5 the relation of $\Delta f/f_0$ and the cavity thickness c is shown for a cavity of Cu/BM with the dimensions $a \times b = 3.2\text{mm} \times 12\text{mm}$.

As shown in Fig. 3, peaks in a resonant curve are weak for a thin cavity because of the energy dissipation due to cavity walls. A possible thickness to be realized by a usual metallization process is about $5\mu\text{m}$, but this is the limit where the resonant curve has an apparent peak (see Fig. 3). A thicker cavity wall is desired to improve the cavity feature and if a thickness over $10\mu\text{m}$ is possible, the jitter $\Delta f/f_0$ is less than 0.02 (see Fig. 5) and the clock frequency can be controlled with precision. On the other hand, a fabrication technique of $10\sim 100\mu\text{m}$ scale components has been discussed recently to achieve a high performance assembly [1] and a technical development to form a thick Cu layer is already realized [11]. This is a promising technology to form a thick cavity so as to obtain a high Q factor.

The power consumed in a cavity system is composed by the Joule heat on the walls, P_J , and energy consumption of a driving circuit, P_D . The former Joule heat P_J can be suppressed when a high Q factor is realized. According to the definition of the Q factor, the Joule heat P_J is represented by $P_J = 2\pi f_0 U/Q$. Using the maximum voltage V_m between the upper and the lower plates of the cavity, the power P_J is expressed by

$$P_J = \frac{\pi(b^2 + n^2 a^2)V_m^2}{16Qf_0 abc}. \quad (5)$$

On the other hand, the driving power P_D is caused by currents to charge and discharge a part of the cavity around a distance of a half wave length away from the driving point. The capacitance of this driving area can be estimated by $C = \varepsilon\pi(\lambda/4)^2/c$ and the driving current becomes $I_D = CV_m f_0 = \pi V_m / 16\mu c f_0$. Assuming that the source voltage is V_{DD} , the power P_D is expressed

$$P_D = \frac{\pi V_{DD} V_m}{16\mu f_0 c}. \quad (6)$$

The total power P defined by $P = P_J + P_D$ decreases when the thickness c becomes large as shown in Fig. 5, where $V_m = 60\text{mV}$, $V_{DD} = 1\text{V}$, $n = 3$ and the cavity dimensions are $a \times b = 3.2\text{mm} \times 12\text{mm}$. According this expression, a thick cavity is effective to suppress the energy consumption because an electric field and capacitance of a cavity are reciprocally proportional to the thickness c .

C. Via array as Cavity Wall

The wave length in a cavity is about 3mm , which is hundred times larger than the size of inter-layer vias. Therefore, the vertical cavity wall can be formed by an array of via pillars. In this section we shows via pillars can reflect the electro-magnetic wave with almost the same efficiency if the via spacing is small.

Figure 6 shows a contour plot of an electric field injected from the negative side of the y -axis. Dashed lines are cross section of via pillars, which are squares with a side of $R_{\text{via}} = 20\mu\text{m}$ and the spacing of $L_{\text{via}} = 50\mu\text{m}$. These sizes are determined from data in [11]. The electric field penetrates through the via spacing, but the field decreases exponentially and the energy transmission scarcely occurs. The electric field \mathbf{E} is polarized along the z -axis and expressed by $\mathbf{E}=(0,0,\Phi(x,y)e^{-i\omega t})$. The field component $\Phi(x,y)$ satisfies

$$\left(\frac{\partial^2}{\partial x^2} + \frac{\partial^2}{\partial y^2} \right) \Phi + V_{sc}(x,y)\Phi + \omega^2 \varepsilon \mu \Phi = 0, \quad (7)$$

where $V_{sc}(x,y)$ is a sort of scattering potential defined by

$$V_{sc}(x,y) = \begin{cases} -\omega^2 \varepsilon \mu + i\omega \mu \sigma & (\text{in via region}) \\ 0 & (\text{in other region}) \end{cases}, \quad (8)$$

with conductivity of via material σ . A solution which satisfies the boundary condition

$$\Phi(x,y) = \begin{cases} e^{ik_0 y} + \sum_p r_p e^{i(G_p x - k_p y)} & (y < 0) \\ \sum_p t_p e^{i(G_p x + k_p y)} & (y > R_{\text{via}}) \end{cases}, \quad (9)$$

is shown in the Fig. 6 where $k_p = (\omega^2 \varepsilon \mu - G_p^2)^{1/2}$, $G_p = 2\pi p/L$ and $L = R_{\text{via}} + L_{\text{via}}$. A detail to obtain this solution is summarized in Appendix C.

If the wave vector k_p is an imaginary number, the wave is localized near the via region. The input wave $\exp(ik_0 y)$ is scattered by the via array and the scattered waves are localized near the via array except a wave with the wave vector of k_0 . The mode conversion between a uniform input wave and the modulated wave along the x -axis does not occur because the wave number of the input wave and the typical Fourier

component of scattering potential $V_{sc}(x,y)$ are quite different in order of magnitude. The variance due to long-range displacement of cavity wall will cause the modulation but the short-range structural modulation such as via array does not generate modulation to the reflection wave.

The magnetic field is obtained by the formula $\mathbf{H} = \nabla \times \mathbf{E} / i\omega$, and the energy flow is expressed by the Poynting vector $\mathbf{E} \times \mathbf{H}$. When the Poynting vector is averaged over the x -axis and time domain, only the y -component remains. This component has the following forms,

$$S_{in} = \frac{1}{2\eta}, \quad (10)$$

$$S_{rf} = \frac{1}{2\omega\mu} \sum_p |r_p|^2 k_p, \quad (11)$$

$$S_{tr} = \frac{1}{2\omega\mu} \sum_p |t_p|^2 k_p \quad (12)$$

for input, reflection and transmission waves, respectively. Here, η is defined by $\eta = (\mu/\epsilon)^{1/2}$. The reflection rate R and transmission rate T are defined by $R = S_{rf}/S_{in}$ and $T = S_{tr}/S_{in}$, respectively.

The quantity $1-R$ indicates the energy loss composed by the Joule heat generated in the via pillar and transmission energy pass through the via spacing. In Fig. 7 the relation between the energy loss $1-R$ and the via spacing L_{via} is shown. The frequency of the input wave is 30GHz, and the square via is made by copper with a size of $R_{via} = 20\mu\text{m}$ a side. If the spacing of vias vanishes and the array turns to be a continuum wall, then, the value of $1-R$ becomes $4R_s/\eta$, where R_s is the sheet resistance defined by $R_s = 1/\delta\sigma$ [12]. An arrow settled at the vertical axis of Fig. 7 indicates this value. If the spacing L_{via} is less than $50\mu\text{m}$, the energy loss $1-R$ is almost the same to that of a continuum wall. Therefore, the via array can be used instead of a continuum wall.

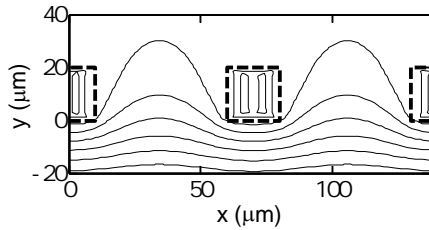


Fig. 6. The contour plot of field strength near via array when the frequency is $f = 30\text{GHz}$. The dashed lines show fringe of via whose size and space are $R_{via} = 20\mu\text{m}$ and $L_{via} = 50\mu\text{m}$, respectively.

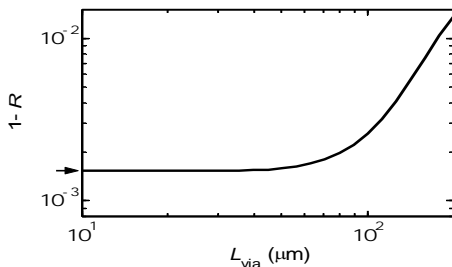


Fig. 7. Relation between the energy loss $1-R$ of reflected flux and the via spacing L_{via} for a via array of the size $R_{via} = 20\mu\text{m}$ when the frequency is $f = 30\text{GHz}$. An arrow in the vertical axis shows the value of $4R_s/\eta$, which is energy loss caused by a continuum wall.

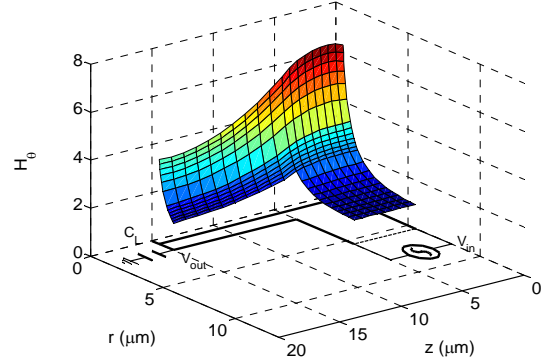


Fig. 8. The magnetic field strength H_θ in a coaxial lead line when the inner and external radii are $0.5\mu\text{m}$ and $1.5\mu\text{m}$, respectively, and the length is $10\mu\text{m}$. A load capacitance $C_L = 30\text{fF}$ is connected at a backend of a lead line.

D. Field in Lead Line

The clock signal is transferred from the cavity to IP blocks on the substrate through leads of a coaxial line. A schematic structure of a lead is shown in Fig. 1 (b), where each terminal is connected to a cavity body and/or a signal gate on a substrate. A typical dimension of a coaxial lead line is about $1\mu\text{m}$ in diameter and $10\mu\text{m}$ in length. Because its dimension is very small and the signal transfer is strongly influenced by the energy dissipation due to Joule heat on the metallic walls, we analyzed the field distribution in the lead line [8].

In Fig. 8 a magnetic field is shown for a lead line of the cylindrical symmetry, where the vertical axis is the angular component H_θ of a magnetic field and the horizontal axis is radius vector r . In the horizontal rz -plane a cross section of the lead is shown, which has dimensions of $0.5\mu\text{m}$ in inner radius, $1.5\mu\text{m}$ in external radius and $10\mu\text{m}$ in length. At the backend a load capacitance $C_L = 30\text{fF}$ is connected, which is a typical gate capacitance of a MOS transistor. The other end is connected to the top plate of a cavity body with a thickness of $5\mu\text{m}$, which is a limiting thickness of an apparent resonant peak.

Although the field distribution is influenced by the energy dissipation, it is confirmed that the signal field penetrates into the end of the lead line. The gain G is defined by the ratio of V_{out}/V_{in} , where the driving voltage V_{in} is applied between the upper and the lower plates of the cavity and the output signal V_{out} is the voltage appeared between the terminals of a load C_L . Using the field distribution shown in Fig. 8, the gain G becomes 0.3 in magnitude and 1.8° in phase angle, which is a sufficient value to transfer the signal.

IV. CONCLUSION

We proposed a novel method using a cavity to distribute a

high-frequency clock over 10GHz. Although the resonance in the cavity is influenced by the Joule heat due to induced current on the cavity walls, the resonant curve has an apparent peak when the thickness is larger than 5 μ m. If the cavity thickness over 10 μ m is possible, the jitter will be suppressed to less than 1/50 of the clock frequency.

In this paper we have mainly discussed clock frequencies near 30GHz. In principle, the clock of higher frequencies can be delivered by our cavity system. For example, a discussion over 100GHz is made, where the cavity meets the requirement to take a clover shape configuration [14].

Recently, a high-performance assembly or packaging has been discussed to enhance the system efficiency of ULSI with use of three-dimensional (3D) interconnections including the process of a backend of the line [1,11]. If the proposed system is implemented into an upper-level interconnect layer, the requirement for a cavity system will be sufficiently satisfied and the clock delivery of a high precision will be possible.

APPENDIX

A. Cavity Oscillation as a Damping Oscillator

A cavity driven by an external current source can be mapped into a damping oscillator with in a framework of FEM of the Galerkin method. By use of this mapping we will derive expressions for the Q factor and the peak width of the resonant curve.

The Galerkin method is a typical technique to discuss electro-magnetic phenomena in the area of FEM [15]. Because the induced currents are related with the magnetic field at the cavity walls, a magnetic field \mathbf{H} is chosen as a field variable. The Galerkin method is a formulation to determine the field \mathbf{H} by seeking a stagnation value of a functional $F[\mathbf{W}, \mathbf{H}]$ defined by

$$F = \int_V [(\nabla \times \mathbf{W}) \cdot (\nabla \times \mathbf{H}) - \varepsilon\mu\omega^2 \mathbf{W} \cdot \mathbf{H}] dV + \int_S \mathbf{W} \cdot \frac{i\omega\varepsilon(1+i)}{\sigma\delta} \mathbf{H} dS - \int_{\Gamma_{ex}} \mathbf{W} \cdot \frac{i\omega\varepsilon(1+i)}{\sigma\delta} \mathbf{J}_{ex} \times d\mathbf{S}. \quad (\text{A1})$$

with respect to an arbitrary field \mathbf{W} . Here, ω is an angular frequency of a driving current, ε and μ are the dielectric constant and the permeability of a filler, V is the volume of the region enclosed by cavity walls and S is the surface region of V . The vector \mathbf{J}_{ex} is a driving current injected from region Γ_{ex} on a cavity wall. The cavity wall is made by a metal with a conductivity σ and its skin depth δ is defined by $(2/\omega\sigma\mu)^{1/2}$. The normal vector \mathbf{n} is toward the external side of the volume V . The vector and the scalar area elements are associated with $d\mathbf{S} = \mathbf{n}dS$. The second term in the left hand side of (A1) is a newly introduced term caused by energy dissipation at the cavity wall.

Taking a variance of F with respect to \mathbf{W} , we obtain

$$\delta F = \int_V \delta \mathbf{W} \cdot \{ \nabla \times (\nabla \times \mathbf{H}) - \omega^2 \varepsilon \mu \mathbf{H} \} dV + \int_S \delta \mathbf{W} \cdot \{ (\nabla \times \mathbf{H}) \times \mathbf{n} + \frac{i\omega\varepsilon(1+i)}{\sigma\delta} \mathbf{H} \} dS - \int_{\Gamma_{ex}} \delta \mathbf{W} \cdot \{ (\nabla \times \mathbf{H}) + \frac{i\omega\varepsilon(1+i)}{\sigma\delta} \mathbf{J}_{ex} \} \times d\mathbf{S}. \quad (\text{A2})$$

If the energy dissipation on cavity walls is neglected, the resonant field \mathbf{H}_0 satisfies the following relation,

$$\int_V \delta \mathbf{W} \cdot \{ \nabla \times (\nabla \times \mathbf{H}_0) - \omega^2 \varepsilon \mu \mathbf{H}_0 \} dV + \int_S \delta \mathbf{W} \cdot (\nabla \times \mathbf{H}_0) \times d\mathbf{S} + \int_{\Gamma_{ex}} \delta \mathbf{W} \cdot (\nabla \times \mathbf{H}_0) \times d\mathbf{S} = 0. \quad (\text{A3})$$

With an assumption that the field in (A1) is given by $\mathbf{H} = \mathbf{H}_0 \xi$ with a time dependent parameter ξ and the subtraction of (A3) from (A2) we obtained the relation as follows,

$$(\omega_0^2 - \omega^2) \varepsilon \mu \xi \int_V \delta \mathbf{W} \cdot \mathbf{H}_0 dV + \xi \int_S \frac{i\omega\varepsilon(1+i)}{\sigma\delta} \delta \mathbf{W} \cdot \mathbf{H}_0 dS = \int_{\Gamma_{ex}} \frac{i\omega\varepsilon(1+i)}{\sigma\delta} \delta \mathbf{W} \cdot \mathbf{J}_{ex} \times d\mathbf{S}. \quad (\text{A4})$$

Because the vector field $\delta \mathbf{W}$ is arbitrary, we can chose $\delta \mathbf{W} = \mathbf{H}_0^*$. Then, the parameter ξ is given by

$$\xi = \frac{(\omega / \omega_0)^{3/2} f_{ex}}{\{1 - (\omega / \omega_0)^2\} + (\omega / \omega_0)^{3/2} (1 - i) / Q}. \quad (\text{A5})$$

Here, Q is the Q -factor defined by

$$Q = \frac{U \omega_0}{P_J} \quad (\text{A6})$$

with U the energy stored in the cavity and P_J the dissipation energy per unit time. The quantity f_{ex} is a driving term due to the external current \mathbf{J}_{ex} . These quantities are defined by

$$P_J = \frac{1}{2} \int_S \sqrt{\frac{\omega_0 \mu}{2\sigma}} \mathbf{H}_0^* \cdot \mathbf{H}_0 dS, \quad (\text{A7})$$

$$U = \frac{\mu}{2} \int_V \mathbf{H}_0^* \cdot \mathbf{H}_0 dV, \quad (\text{A8})$$

$$f_{ex} = \frac{1+i}{2U\omega_0} \int_S \sqrt{\frac{\omega_0 \mu}{2\sigma}} \mathbf{H}_0^* \cdot \mathbf{J}_{ex} \times d\mathbf{S}. \quad (\text{A9})$$

The parameter ξ reaches its peak when the driving frequency becomes ω_R , which is given by

$$\frac{\omega_R}{\omega_0} \approx 1 - \frac{1}{2Q} + \frac{1}{4Q^2} \quad (\text{A10})$$

and the peak value satisfies $|\xi f_{\text{ex}}|^2 \approx Q^2$. The width of the peak $\Delta\omega_R$ is defined by the interval of points where the amplitude becomes half of the peak value, i.e. $|\xi f_{\text{ex}}|^2 \approx Q^2/2$. The resultant expression derived from this definition is;

$$\frac{\Delta\omega_R}{\omega_0} \approx \frac{2}{Q} + \frac{7}{4Q^3}. \quad (\text{A11})$$

The relation between the jitter Δf and the Q factor given by (4) is defined by $\Delta f/f_0 = (\Delta\omega_R/\omega_0)/4$. The relation (3) and (5) is derived from the definition of Q , P_j and the resonant wave:

$$\begin{aligned} \mathbf{H}_0 &= A_m \left(\sin\left(\frac{\pi x}{a}\right) \cos\left(\frac{\pi x}{b}\right), 0, \cos\left(\frac{\pi x}{a}\right) \sin\left(\frac{\pi x}{b}\right) \right) \cos(\omega t), \\ \mathbf{E}_0 &= A_m \frac{a\omega\mu}{\pi} \left(0, \sin\left(\frac{\pi x}{a}\right) \sin\left(\frac{\pi x}{b}\right), 0 \right) \sin(\omega t). \end{aligned} \quad (\text{A12})$$

Here, the maximum amplitude A_m of the magnetic field is expressed with the maximum voltage V_m between the upper and lower plates as $A_m = V_m/2f_0\mu\epsilon a$.

B. Effective Sheet Resistance of Double-Layered Wall

Assuming that the cavity wall is formed with a main metal of a conductance σ_M and a barrier metal of conductance σ_B , we derive an effective sheet resistance of the double-layered wall. The electric field in a perfect metal has no component perpendicular to the surface and a parallel component E . When the field is oscillating by a frequency *i.e.* $E(z,t) = E_s(z)e^{i\omega t}$, the field E satisfies

$$\frac{d^2 E}{dz^2} = \begin{cases} i\omega\sigma_B\mu E & (0 < z < d) \\ i\omega\sigma_M\mu E & (d < z) \end{cases}, \quad (\text{B1})$$

where the z -axis is taken perpendicular to the surface and d is the depth of the barrier metal. Solving the equation (B1) with the boundary conditions that the field and its derivative at the interface $z = d$ are continuous, we obtained the expression for the space domain as follows,

$$E_s = \begin{cases} C[(1+r)e^{\gamma_B(z-d)} + (1-r)e^{-\gamma_B(z-d)}] & (0 < z < d) \\ Ce^{-\gamma_B(z-d)} & (d < z) \end{cases}, \quad (\text{B2})$$

where $\gamma_B = (1+i)/\delta_B$, $r = (\sigma_M/\sigma_B)^{0.5}$ and the constant C is related with the electric field $E_p (= E_s(0))$ as follows,

$$E_p = C[(1+r)e^{\gamma_B d} + (1-r)e^{-\gamma_B d}]. \quad (\text{B3})$$

The constant C is also associated to the parallel component H_p of the magnetic field at the surface to the total current by the following relation:

$$H_p = \int_0^d \sigma_B E dz + \int_d^\infty \sigma_M E dz. \quad (\text{B4})$$

The power of the Joule heat is expressed with the real part $E_r = \text{Re}[E]$ as follows,

$$P = \int_0^d \sigma_B E_r^2 dz + \int_d^\infty \sigma_M E_r^2 dz. \quad (\text{B5})$$

Defining an effective sheet resistance R_{eff} by $P = R_{\text{eff}} H_p^2/2$, we obtain the expression (2).

C. Scattering Formulation for Reflection from Via Array

The partial differential equation (8) for the scattering wave can be reduced to an ordinary differential equation by use of a Fourier transformation along the x -axis. A numerical solution of this ordinary differential equation can be obtained by use of a difference equation of second order. This formulation is developed in the area of solid-state physics [16]. We are modulated this scattering formalism for the purpose to analyze the electro-magnetic wave.

When the wave $\Phi(x,y)$ is transformed to Fourier series as $\Phi(x,y) = \sum_p \phi_p(y) \exp(iG_p x)$, the equation (8) is reduced to follows,

$$\frac{d^2}{dy^2} \phi_p + \sum_q [v_{p-q} + (\omega^2 \epsilon \mu - G_p^2) \delta_{pq}] \phi_q = 0, \quad (\text{C1})$$

where $v_p(y)$ is the Fourier transformation of (9) with respect to x -axis and G_p is a wave number defined by $G_p = 2\pi p/L$ with $L = R_{\text{via}} + L_{\text{via}}$. Introducing a state vector $\Psi(y) = \{\phi_p(y)\}$ and a matrix $\mathbf{V}(y) = [v_{p-q} + (\omega^2 \epsilon \mu - G_p^2) \delta_{pq}]$, the equation (C1) can be expressed by

$$\frac{d^2}{dy^2} \Psi + \mathbf{V} \Psi = 0. \quad (\text{C2})$$

We use discrete coordinate along y -axis defined by $y = hn$ ($n = 0, 1, 2, \dots, N$) with an interval h and introducing a scattering matrix S_n defined by

$$\Psi(hn+h) = S_n \Psi(hn). \quad (\text{C3})$$

Then, the equation (8) is transformed into a difference equation such as

$$S_{n-1} = -(a_n S_n + b_n)^{-1} c_n, \quad (\text{C4})$$

where the matrix a_n, b_n and c_n are defined by

$$a_n = I + \frac{h^2}{12} \mathbf{V}(hn+h), \quad (\text{C5})$$

$$b_n = -2I + \frac{5h^2}{6} \mathbf{V}(hn), \quad (\text{C6})$$

$$c_n = I + \frac{h^2}{12} \mathbf{V}(hn-h), \quad (\text{C7})$$

with the unit matrix I .

By use of the matrix S_n and the state vector $\Psi(hn)$, the boundary condition (9) is expressed as,

$$S_n \rightarrow [e^{ik_p h} \delta_{pq}], \quad (n \rightarrow N), \quad (\text{C8})$$

$$\Psi(hn) \rightarrow \Psi_{\text{in}} + \Psi_{\text{rf}}, \quad (n \rightarrow 0), \quad (\text{C9})$$

with a wave number $k_p = (\omega^2 \epsilon \mu - G_p^2)^{1/2}$, an input vector $\Psi_{\text{in}} = \{\delta_{p0}\}$ and a reflection vector $\Psi_{\text{rf}} = \{r_p\}$.

Using the relation (C4) and the condition (C8), all matrices S_n are determined recursively from $S_N (= [e^{ik_p h} \delta_{pq}])$. All state vectors $\Psi(nh)$ are obtained successively from $\Psi(0) (= \Psi_{\text{in}} + \Psi_{\text{rf}})$ by use of the condition (C9) and the relation (C3). The reflection vector Ψ_{rf} and transmission vector $\Psi_{\text{tr}} = \{t_p\}$ are expressed as follows,

$$\Psi_{\text{rf}} = -(S_0 - K_+)^{-1} (S_0 - K_-) \Psi_{\text{in}}, \quad (\text{C10})$$

$$\Psi_{\text{tr}} = K_-^N S_{N-1} \cdots S_2 S_1 S_0 (\Psi_{\text{in}} + \Psi_{\text{rf}}), \quad (\text{C11})$$

where $K_+ = [e^{ik_p h} \delta_{pq}]$ and $K_- = K_+^{-1}$. The energy flux of (11) and (12) can be obtained by use of (C10) and (C11).

REFERENCES

- [1] T. Sakurai, "System-on-a-chip vs. system-in-a-package: design and interconnection issues", in Proc. of Advanced Metallization Conf. 2003, MRS Warrendale PA 2004, pp.3-10.
- [2] H. Shinoki, H. Ito, Y. Yokoyama and K. Masu, "Transmission line interconnect structure in Si ULSI", in Dig. of Advanced Metallization Conf. 2002: Asian Session, Tokyo, Japan, pp.78-79.
- [3] K. Kim, W. Bomstad and K. K. O, "A plane wave model approach to understanding propagation in an intra-chip communication system", in Dig. of IEEE Antennas & Propagation Society, International Symposium 2001, Boston MA, vol.2, pp.166-169.
- [4] S. Watanabe, A. B. M. H. Rashid and T. Kikkawa, "Influence of Si substrate ground in antenna transmission gain for on-chip wireless interconnect", Dig. of Advanced Metallization Conf. 2002: Asian Session, Tokyo, Japan, pp.94-95.
- [5] K. M. Kurisu, "Instrument on a semiconductor LSI and clock delivering method", Japanese patent, PAT No. 2998690., April 30, 1997.
- [6] P. Kapur and K. C. Saraswat, "Power dissipation in optical clock distribution network for high performance ICs", in Proc. of IEEE 2002 International Interconnect Techn. Conf., San Francisco CA, pp.151-153.
- [7] H.Kato, E. Kondoh, T. Akitsu, T. Kohori and H. Morishita, "Noise free and jitter-less clock distribution method for high-frequency system using microcavity" in Proc. of Advanced Metallization Conf. 2003, MRS Warrendale PA 2004, pp.65-68.
- [8] T. Kohori, H.Kato, E. Kondoh, T. Akitsu, "Features of microcavity to distribute high-frequency clock over than 10GHz", in Dig. of Advanced Metallization Conf. 2004:Asian Session, Tokyo Japan, pp.96-97. .
- [9] F. O'Mahony, C. Yue and S. Wong, "10GHz Clock Distribution Using Coupled Standing-Wave Oscillators", in Dig. of IEEE Int. Solid State Circuits Conf. 2003, San Francisco CA, pp. 428-429 ; IEEE Journal of Solid State Circuits, Vol.38, Nov. 2003, pp. 1813-1820.
- [10] D. Ham and W. Andress, "A circular standing wave oscillator", in Dig. of IEEE Int. Solid-State Circuits Conf. 2004, San Francisco CA, pp.380-381.
- [11] K. Kikuchi, M. Takamiya, Y. Kudoh, K. Soejima, H. Honda, M. Mizuno and S. Yamamichi, "A package-process- oriented multilevel 5 μm -thick Cu wiring technology with pulse periodic reverse electroplating and photosensitive resin" in Proc. of IEEE International Interconnect Tech. Conf. 2003, San Francisco CA, pp.189-191.
- [12] S. Ramo, J. R. Whinnery and T. Van Duzer, *Fields and waves in communication electronics (Third Edition)*, New York: Jon Wiley & Sons Inc., 1994.
- [14] H. Kato, T. Kohori, K. Watanabe, Y. Kodaira, E. Kondoh, T. Akitsu and H. Kato, "How to deliver a high-frequency clock over 100GHz using BEOL technologies", in Dig. of Advanced Metallization Conference 2005:Asian Session, Tokyo Japan, pp.110-111.
- [15] M. Koshiha, *Introduction to finite element method for optics and waves*, Tokyo, Morikita Shuppan Co., 1990, p.11.
- [16] K. Hirose and M. Tsukada, "First-principles calculation of the electronic structure for a bielectrode junction system under strong field and current", Physical Review B, vol. 51, no. 8, Feb. 1995, pp.5278-5290.

Hatsuhiko Kato received a PhD degree from Hokkaido University, Sapporo, Japan in 1987 and he joined the ULSI Research Center, Toshiba Ltd., Kawasaki, Japan, where he was engaged in research of high-speed SRAM's including BiCMOS technology. After he transferred to Hakodate National College of Technology and spending at Antwerpen University, he has been working in the University of Yamanashi since 1999. He is a member of the Institute of Electronics, Information and Communication Engineers and the Physical Society of Japan.

Takaya Kohori received a B.S. degree from the University of Yamanashi in 2003 and he is currently working toward a M.S. degree in the graduate school of the University of Yamanashi, Kofu Japan.

Eiichi Kondoh obtained his BE and ME degrees from Waseda University, and a Ph.D. from Kyoto University all in materials science. He has experience in R&D for thin films processing at Kawasaki Steel, the Max-Planck Institute, and IMEC. Since 1998 he holds professorship and is now with the Graduate School of the University of Yamanashi, Japan. He is a member of Japan Society of Applied Physics, Japan Institute of Metals, American Vacuum Society, and Electrochemical Society.

Tetsuya Akitsu received a Doctor (Eng.) degree from Kyoto University, Kyoto, Japan. He was working on low temperature plasma and applications at the University of Yamanashi, Faculty of Engineering, and later the Interdisciplinary Graduate School of Medicine and Engineering, since 1982. He is a member of the IEEE, Tokyo Branch, The Japan Society of Plasma Science and Nuclear Fusion on Research, Japanese Applied Physics Society, Japanese Institute of Electrical Engineering, and the directors board of the Bio-Material Society Japan.

Hatsuyoshi Kato is a professor in physics at the Tomakomai National College of Technology in Japan. He holds a PhD in applied physics from Hokkaido University in Sapporo Japan, and has studied phonon properties of layered elastic media at Brown University in Rhode Island. Previously, he was with NEC Corp. working in CAD systems for logic and fault simulation and logic synthesis for VLSI chips. He is a member of the Physical Society of Japan.